Available online at www.sciencedirect.com
SCIENCE DIRECT®
Acta Materialia 53 (2005) 1167–1178
Acta MATERIALIA
www.actamat-journals.com

Role of particle size and filler–matrix adhesion on dynamic fracture of glass-filled epoxy. II. Linkage between macro- and micro-measurements

R. Kitey, H.V. Tippur *

Department of Mechanical Engineering, Auburn University, 202 Ross Hall, Alabama 36849, USA

Received 30 April 2004; received in revised form 4 November 2004; accepted 5 November 2004
Available online 10 December 2004

Abstract

Spherical particles of mean diameter 7–200 μm are used to reinforce epoxy matrix at a constant volume fraction (10%) and two different filler–matrix strengths, weak and strong. Role of particle size and filler–matrix adhesion strength on steady-state dynamic fracture toughness is investigated by linking optical measurements reported in [1] with surface roughness parameters. Crack tilting and twisting appears to dominate when filler is strongly bonded to the matrix while crack front twisting and blunting occur with weakly bonded filler. The weaker filler–matrix interfaces also act as distributed attractors of a propagating crack resulting in greater surface roughness. A linear relationship between fracture toughness and surface roughness is seen when particle size effects and filler–matrix adhesion effects are factored out. The overall surface roughness (Ra) does not correlate with macro-measurements and only a component of Ra, defined as "fracture induced roughness", Ra_f does. A model for calculating Ra_f based on volume fraction, particle size, inter-particle spacing and overall surface roughness is introduced. A linear relationship between steady state fracture toughness and the quantity $Ra_f/\sqrt{D}$ (D being the average particle diameter) has been found to exist.

Keywords: Particulate composites; Matrix reinforcement; Dynamic fracture; Micromeasurements; Surface roughness; Crack growth mechanisms

1. Introduction

In part I of this study [1], the effects of particle size and filler–matrix adhesion strength on macroscopic fracture parameters have been quantified. Particle size as well as filler–matrix adhesion strength have been shown to influence the dynamic crack initiation and growth in glass-filled epoxies. Strengthening mechanisms such as crack deflection, crack-tip blunting, crack front twisting have been identified as a few probable reasons behind the differences seen in macroscopic fracture parameters. The experimental results do not show a monotonic relation between particle size and fracture toughness. Therefore investigating alternative micro-parameters to explain the phenomena is essential.

It is recognized that fracture parameters leave an imprint on the fracture surfaces created during failure. Thus, fracture surface morphology can be used as a fingerprint for understanding the mechanics of fracture by performing various micro-measurements. In conventional homogeneous materials it is seen that crack velocity and stress intensity factors have considerable effect on microscopic features such as surface roughness, average roughness slope. It is widely recognized that the increase in crack velocity or fracture toughness increases the surface roughness in conventional monolithic materials. But qualitative and quantitative understanding of surface parameters become complicated when secondary

* Corresponding author. Tel.: +1 334 844 3327; fax: +1 334 844 3307.
E-mail address: htippur@eng.auburn.edu (H.V. Tippur).

1359-6454/$30.00
doi:10.1016/j.actamat.2004.11.011

phases of various size, shape and volume fraction come into the picture in heterogeneous materials. Mechanisms such as crack deflection, twisting, microcracking, bridging or crack tip blunting, which dominate failure processes in heterogeneous materials, could have an immense effect on energy dissipation and hence fracture surface morphology.

The effects of crack velocity and/or stress intensity factor on surface roughness is widely recognized and studied in monolithic materials. Cottrell's [2] work on PMMA (poly methyl methacrylate) has shown that surface roughness increases with crack velocity. Ravichandar and Knauss [3] have also shown consistent increase in surface roughness with stress intensity factor for Homilite-100. Arakawa et al. [4], [5] have studied the effects of dynamic stress intensity factor on various roughness parameters for PMMA, Homilite-100 and Epoxy (Araldite-B). They have reported an increase in surface roughness with crack velocity. However, they have found crack velocities not to be uniquely related to surface roughness due to differences stemming from crack accelerations and deccelerations. They identified that surface roughness correlates better with $R^*\dot{a}$ ($\dot{a}$ being crack velocity, $R^*\dot{a}$ being the specific crack extension resistance) than other fracture parameters. Further, they have also shown a qualitative relation between average RMS roughness value with crack velocity and dynamic stress intensity factor with some discrepancies. Sharon et al. [6] have measured energy flux into the tip of a dynamically moving crack and the total surface area created due to microbranching in PMMA. They have demonstrated that the total surface area, resulting from the generation of microbranches above the critical crack velocity, increases linearly with energy flux.

Among the studies on heterogeneous materials, a significant body of literature is on cementitious materials. Tandon and Faber [7] have studied the effect of loading rate on the fracture behavior of cement paste, mortar and concrete. They show a qualitative relationship between fracture toughness and surface roughness by noting that with an increase in loading rate both fracture toughness and surface roughness increase. Using fractal dimensions to correlate fracture and surface roughness parameters in concrete has been suggested by Issa et al. [8]. They have used aggregates of different maximum sizes varying from 10 to 70 mm in their study. They have been able to show that *modified* fracture energy and fractal dimension could be fitted with similar logarithmic functions. Further a linear relation between fractal dimension and modified fracture energy has been suggested. But this relation is found to depend on specimen geometry because the fractal dimension and the modified fracture energy depend on specimen size. Abell and Lange [9] have taken a different approach to relate fracture and roughness parameters. They have used confocal laser microscopy and video density technique to characterize surface geometry of cementitious material. They have calculated toughening ratio in the presence of aggregates by using crack deflection model proposed by Faber and Evans [10,11]. A relationship between toughening ratio and roughness number has been shown by fitting data for linear elastic materials. They report that fracture behavior of cementitious materials increasingly deviates from linear elastic behavior as surface roughness increases.

Among the very few works on non-cementitious materials with microsize fillers, Davidson [12] has reported experimental results of fracture toughness and roughness parameters for silicon carbide reinforced aluminium alloy particulate composite ($V_f - 15\%$ and 25%). He has analyzed various fracture parameters like surface roughness ratio coefficient, profile roughness factor coefficient and fractal dimensions from fractured surfaces. None of these parameters have been found to correlate with fracture toughness satisfactorily. He has attributed this to very little work being expended in the formation of new surfaces compared to plastic dissipation in the matrix.

Other than the approaches involving fractal dimensions and the roughness parameters reviewed above, few other methods have also been successfully used in past to correlate micro- and macro-measurements. Kobayashi and Shockey [13,14] have demonstrated that fracture surface topography analysis can assess the fracture toughness, crack nucleation time and crack growth history. Fourier power spectrum is another method in this regard, which has also been used in many other applications. Komai et al. [15] have used Fourier power spectrum to recognize striations and intergranular failure by measuring regularity, directionality and coarseness of an image. Hao et al. [16] have applied Fourier transform method to study fatigue fracture surfaces of commercial aluminum. They demonstrated that the exponent index in curve fitting of power spectrum peaks reflects the change in fatigue crack propagation rate and is inversely related to power spectrum. Kobayashi and Shockey [17] have correlated elevation power spectrum density curve with load parameters, stress intensity range and stress ratio by using FFT analysis on fatigue fracture surface topography of a titanium alloy.

As can be seen in the review of the literature above, correlation of micro- and macro-fracture parameters is yet to be achieved satisfactorily, particularly for heterogeneous materials. This is attributed to the fact that micro-measurements are relatively complex in heterogeneous material systems due to the presence of secondary phases. Furthermore, most of the studies with secondary phase material has been performed with relatively uncontrolled filler sizes and shapes and mostly in cementitious materials with rather large fillers. Also there is no unique roughness parameter that has been shown to correlate well with fracture toughness. Accordingly, in this paper studies on glass-filled epoxy particu-

late composites with various microscopic filler sizes but of identical shape are reported. The composites studied have macroscopically similar elastic and physical characteristics as well. Surface roughness along with filler particle size are used in correlating macro-measurements with fracture surface parameters.

2. Micro-measurements

2.1. Methodology

Ten percent soda-lime glass spheres were mixed with low viscosity epoxy to cast 8 mm thick sheets. Cast sheets were machined to prepare the test samples of in-plane dimensions 152 mm × 42 mm. To study the particle size effect solid glass spheres of mean diameters 7, 11, 35, 71 and 203 μm were used. Weak and strong filler matrix interfaces were created using uncoated and silane treated particles of above mentioned sizes to study the filler–matrix adhesion effect. Pre-cracked specimens of crack lengths 10 mm were impact loaded at a velocity of 5.3 m/s. The optical method of coherent gradient sensing along with high-speed photography (200,000 fps) has been used to study crack-tip deformations and to evaluate fracture parameters. Detailed information on all the above can be found in part I of this study [1].

Scanning electron microscopy (SEM) was used for qualitative examination of fracture surfaces. Approximately 1.5–2 mm thin strips of fractured surface with cross sectional area 42 mm × 8 mm were stripped out from the fractured sample. Fracture surfaces were deposited with a thin layer of gold using a vacuum evaporator. Various locations in the steady state crack growth region (see [1]) were examined using SEM. Quantitative micro-measurements of fracture surfaces were performed subsequently using a Tencor P-1 long scan profiler with a stylus of root radius of 5 μm. Digitized surface profiles were measured in a region that corresponds to steady state crack growth. It can be noticed from velocity histories in the specimens (see Fig. 4(a) and 7(a) in [1]) that the steady state region falls in the mid one-third along the specimen width. That is, $x = 4$–18 mm ahead of the initial crack tip depending upon the filler particle size. The data was recorded at 4–5 different locations within the steady state region.

2.2. Fracture surface parameters

Fig. 1 shows micrographs of a few representative fractured surfaces. The images are for 203 μm (Fig. 1(a) and (b)), 35 μm (Fig. 1(c) and (d)) and 11 μm (Fig. 1(e) and (f)) weakly bonded and strongly bonded particles, respectively. It is evident from the micrographs that agglomeration effects are essentially nonexistent in these cases. The matrix wetting on filler particles in Fig. 1(b), (d) and (f) suggests strong filler–matrix adhesion in the case of silane coated fillers. Contrary to this, for uncoated particles in Fig. 1(a), (c) and (e), no such affinity between filler and matrix can be seen due to weaker filler–matrix interface. In the case of weakly bonded particles, inter-particle cleavage fracture can be noticed, with either particle or particle footprints left behind on the surface. Relatively higher surface waviness can be seen in strongly bonded particles as the crack appears to have mostly avoided the filler particles and has propagated through the matrix material. Due to this, fewer particles are exposed on the fracture surface. The situation can be imagined as if particles are hidden just below/above a layer of matrix material adjacent to the fracture surface. On the contrary, the larger number of particles and particle footprints in the weakly bonded filler case suggests that there is only a weak resistance to filler–matrix interfacial separation. Highly textured surface in smaller particles suggest higher energy dissipation and hence higher fracture toughness compared to 203 μm particles.

Digitized data from the surface profiler has been processed to get average surface roughness Ra using,

$$\mathrm{Ra} = \lim_{L\to\infty} \frac{1}{L} \int_{-L/2}^{+L/2} |y(x) - \bar{y}|\, \mathrm{d}x, \tag{1}$$

where

$$\bar{y} = \lim_{L\to\infty} \frac{1}{L} \int_{-L/2}^{+L/2} y(x)\, \mathrm{d}x. \tag{2}$$

Here L is the scan length and (x, y) are defined as shown in Fig. 2.

In the presence of filler material, surface profiles could be modeled as shown in Fig. 3. That is, the surface profile can be viewed as a combination of profiles due to particle/cavity and surface roughness due to the fracture process itself. One can consider this to be a sum of particle-related roughness and fracture-induced roughness. The particle-related roughness, $\mathrm{Ra_p}$, is the average surface roughness in the presence of embedded particles without considering disturbances to the surface profile generated by the fracture process. The fracture-induced roughness, $\mathrm{Ra_f}$, on the other hand can be viewed as the average roughness of fractured surface generated due to energy dissipation without considering the filler phase but inclusive of all its manifestations during fracture. Thus, the average surface roughness measured by the profiler can be approximated to be a combination of $\mathrm{Ra_p}$ and $\mathrm{Ra_f}$. Since various mechanisms affecting the fracture toughness of the material are reflected in the fracture-induced surface roughness component, it is appropriate to examine $\mathrm{Ra_f}$ to investigate the effect of particle size and filler–matrix adhesion on macro-scale fracture parameters in particulate composites. The fracture-induced roughness is thus obtained as,

$$\mathrm{Ra_f} = \mathrm{Ra} - \mathrm{Ra_p}. \tag{3}$$

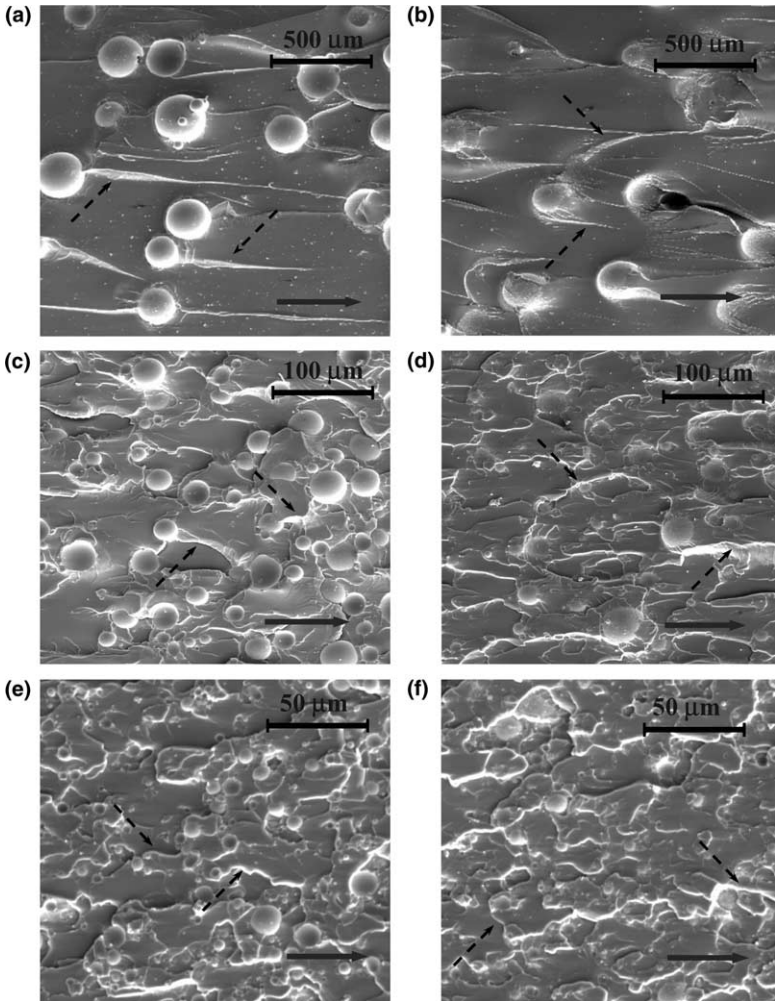

Fig. 1. SEM micrographs: (a) 203 μm uncoated particles, (b) 203 μm coated particles, (c) 35 μm uncoated particles, (d) 35 μm coated particles, (e) 11 μm uncoated particles, (f) 11 μm coated particles. Solid arrow shows crack propagation direction and broken arrow shows "Tail lines".

2.2.1. Particle-related roughness

Let us assume an ideal case of particles being uniformly distributed in the matrix and where the crack interacts with particles exactly at the equatorial sections of particles while propagating through the matrix. Two extreme possibilities of material separation are shown schematically in Fig. 4. First possibility is shown in Fig. 4(a) and (b). Fig. 4(a) corresponds to the situation when all the particles have exited the matrix material during fracture forming cavities while Fig. 4(b) is when all the particles exist on one of the fracture surfaces. A second possibility in Fig. 4(c) shows the case where equal numbers of particles are pulled out or left behind in the matrix during fracture. Clearly these two are limiting cases for particles/cavities on the fracture surface. Average inter-particle separation l for a given volume fraction V_f and an average particle diameter D is given by [18,19],

$$l = \frac{2D(1 - V_f)}{3V_f}. \tag{4}$$

Let us first consider the case corresponding to Fig. 4(a). Surface profile $y(x)$ due to particles/cavities on fracture surface can be simply represented as,

$$y(x) = -\sqrt{(D/2)^2 - x^2}. \tag{5}$$

Hence the average surface profile $\bar{y}$ from Eq. (2),

$$\bar{y} = \frac{1}{Nl}\int_{-Nl/2}^{Nl/2} y(x)\,\mathrm{d}x, \tag{6}$$

where scan length L is replaced by Nl, N being the number of particles within L and l is inter-particle separation as defined earlier. From the schematic it can be seen that $\bar{y} = 0$ between particle footprints, hence average surface profile can further be simplified to

$$\bar{y} = \frac{N}{Nl}\int_{-D/2}^{D/2} y(x)\,\mathrm{d}x. \tag{7}$$

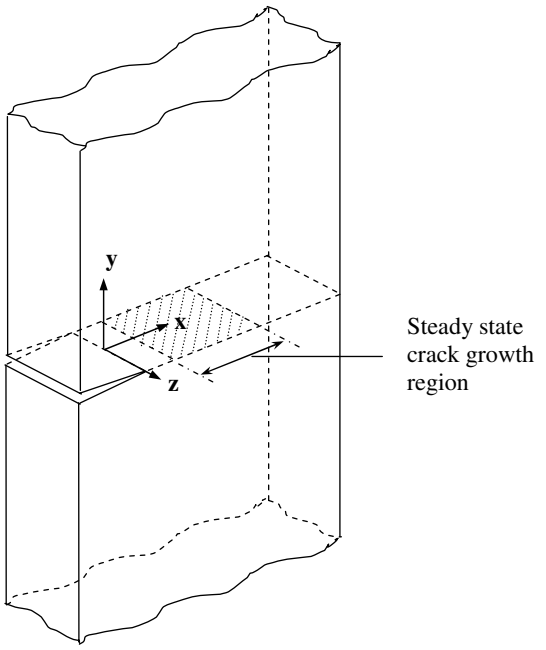

Fig. 2. Schematic representing a growing crack in the composite.

Considering the profile symmetry about y-axis leads to,

$$\bar{y} = \frac{2}{l}\int_0^{D/2} y(x)\,\mathrm{d}x = -\frac{\pi}{2l}(D/2)^2. \tag{8}$$

From Eq. (4) let,

$$\frac{D/2}{l} = \frac{3V_f}{4(1-V_f)} = C, \tag{9}$$

where C is the ratio of particle radius to inter-particle distance and is a function of volume fraction only. Thus from Eqs. (8) and (9),

$$\bar{y} = -\frac{\pi C D}{4}. \tag{10}$$

Now from Eq. (5),

$$x|_{y=\frac{\pi CD}{4}} = \frac{D}{2}\sqrt{1-\left(\frac{\pi C}{2}\right)^2} = \frac{D}{2}\delta, \tag{11}$$

where $\delta = \sqrt{1-(\frac{\pi C}{2})^2}$.

Then from Eq. (1) the particle-related roughness is,

$$\begin{aligned}\mathrm{Ra_p} &= \frac{2}{l}\int_0^{D/2} |y(x)-\bar{y}|\,\mathrm{d}x \\ &= \frac{2}{l}\left\{\int_0^{D\delta/2}(\bar{y}-y(x))\,\mathrm{d}x + \int_{-D\delta/2}^{D/2}(y(x)-\bar{y})\,\mathrm{d}x\right\},\end{aligned} \tag{12}$$

where $L = Nl$ has been utilized again. Upon integration, we get,

$$\mathrm{Ra_p} = \frac{D}{2}C\left\{\frac{\pi}{2}(1+2C-4C\delta) - 2\cos^{-1}\delta + \sin(2\cos^{-1}\delta)\right\}. \tag{13}$$

For $V_f = 10\%$, $C = 0.0833$ and $\delta = 0.9914$. Hence, particle-induced roughness from Eq. (13) is,

$$\mathrm{Ra_p} = 0.0505D. \tag{14}$$

It should be noted that the result in Eq. (14) remains unaltered if Fig. 4(b) were considered. Similarly for the case corresponding to Fig. 4(c), $\bar{y} = 0$ and $\mathrm{Ra_p} = \pi CD/4$. Hence for 10% volume fraction it can be shown that,

$$\mathrm{Ra_p} = 0.0655D. \tag{15}$$

The two cases above show the limiting values of $\mathrm{Ra_p}$. Actual value will be somewhere in between these two, depending upon particle/cavity distribution on the fracture surface. The value of $\mathrm{Ra_p} = 0.0655D$ has been considered as the particle-related roughness for further analysis in this paper. However, the results and conclusions remain unaffected if Eq. (14) is considered instead.

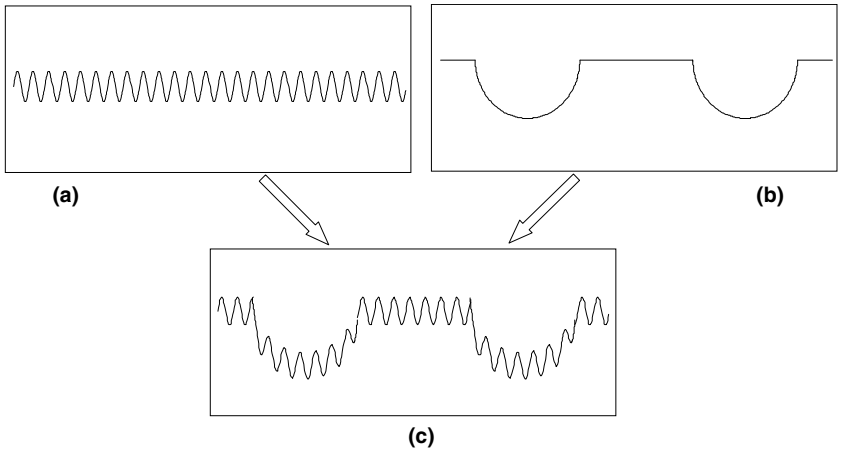

Fig. 3. Schematic showing the effect of embedded particle/particle foot-prints on fracture surface morphology: (a) fracture surface profile excluding embedded particles/particle foot-prints, (b) isolated surface profile due to embedded particles/particle foot-prints and (c) fracture surface profile in the presence of embedded particles/particle foot-prints.

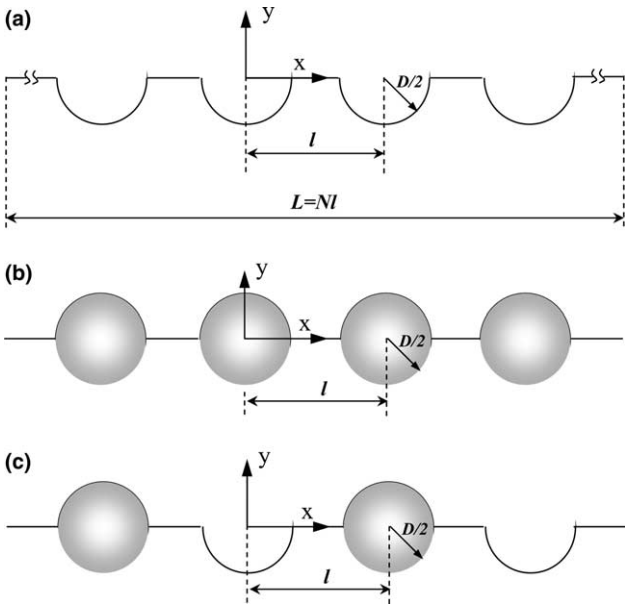

Fig. 4. Schematic representation of fracture surface: (a) in the presence of particle foot-prints, (b) in the presence of particles and (c) in the presence of particles and particle foot-prints.

3. Results and discussions

Fig. 5 shows a few representative surface profiles for weakly and strongly bonded fillers of different particle sizes in the matrix. The profiles shown are for 11, 35 and 203 μm cases to maintain consistency with part I of this work [1]. Each surface profile is qualitatively distinct from the others. In Fig. 5(a) the effects of particle size on surface profiles are compared for weakly bonded case. The largest particle surface profile shows larger amplitudes and longer wavelengths with a relatively small higher frequency content when compared to other particle sizes. The specimen with 11 μm particles, on the other hand, shows substantially higher frequency content with a surface profile generally much closer to the mean surface. That is amplitudes are smaller compared to other particle sizes shown in the plot. Weakly bonded 35 μm particles, which has shown the highest macroscopic fracture toughness among all the cases considered [1], shows a frequency content similar to that of 11 μm particles, while the amplitude is larger, similar to that of 203 μm particles. Next, the surface profiles of coated and uncoated 35 μm are compared in Fig. 5(b). Evidently, the profile for coated case has relatively smaller amplitude when compared to the uncoated case. In Fig. 5(b), surface profile of unfilled epoxy is also shown for comparison. It can be seen that the profile for epoxy is quite close to the mean surface with a relatively small surface amplitude. This suggests a lower surface roughness in the case of unfilled epoxy compared to the filled ones. The effect of these differences in surface profiles can be clearly seen on average surface measurements

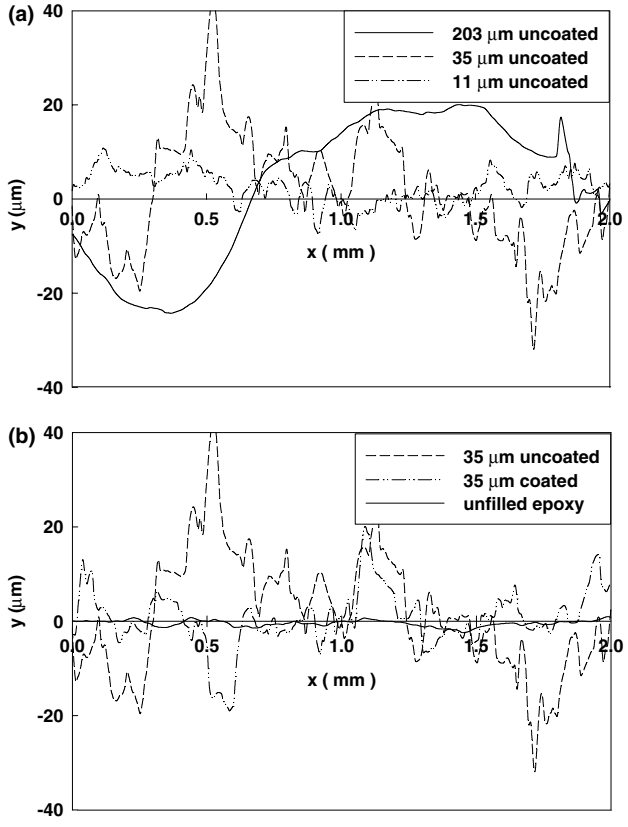

Fig. 5. Representative fracture surface profiles for different glass-filled epoxy specimen with weakly bonded particles showing: (a) particle size effect and (b) filler–matrix adhesion effect.

to be described next. It should be noted that roughness of fractured surfaces has been evaluated for each sample in a region where steady state crack growth is observed. Surface roughness profiles in both x-direction and z-direction are recorded at 4–5 different locations. Surface roughness is calculated using Eq. (1) and the resulting average values are tabulated in Tables 1 and 2 as longitudinal roughness Ra_x and transverse roughness Ra_z, respectively.

3.1. Particle size and filler–matrix adhesion effect

In Table 1 both Ra_x and Ra_z show increasing trend as particle size increases when uncoated (weakly bonded) particles are used to reinforce the matrix. Average roughness Ra has been calculated by geometrically averaging Ra_x and Ra_z. It can be seen from the table that average surface roughness increases with particle size. Also, roughness values are slightly but consistently higher in the transverse direction in all cases. It should be pointed out that average roughness values Ra do not provide a consistent explanation for the fracture toughness variation of the filled material as a function of particle size. This can be seen when micro- and macro-measurements listed in Table 3 are compared. That is,

Table 1
Roughness parameters for weakly bonded glass fillers in epoxy matrix, $V_f = 0.1$

Particle diameter, D (μm)	Longitudinal roughness, Ra_x (μm)	Transverse roughness, Ra_z (μm)	Average roughness, Ra (μm)	Particle-related roughness, Ra_p (μm)	Fracture-induced roughness, Ra_f (μm)	$Ra_f/\sqrt{D}$ ($\sqrt{\mu m}$)
203	16.50	18.80	17.61	11.17	6.44	0.45
71	9.85	9.95	9.90	3.91	5.99	0.71
35	9.63	11.09	10.33	1.93	8.40	1.42
11	3.48	3.57	3.52	0.61	2.91	0.88
7	2.31	2.41	2.36	0.39	1.97	0.75
Epoxy	0.75	0.80	0.77	–	–	–

Table 2
Roughness parameters for strongly bonded glass fillers in epoxy, $V_f = 0.1$

Particle diameter, D (μm)	Longitudinal roughness, Ra_x (μm)	Transverse roughness, Ra_z (μm)	Average roughness, Ra (μm)	Particle-related roughness, Ra_p (μm)	Fracture-induced roughness, Ra_f (μm)	$Ra_f/\sqrt{D}$ ($\sqrt{\mu m}$)
203	16.34	17.78	17.04	11.17	5.87	0.41
35	5.71	6.30	6.00	1.93	4.07	0.69
11	2.36	2.49	2.42	0.61	1.81	0.55

unlike fracture toughness, overall roughness is highest for the largest particle size and monotonically decreases as particle size decreases. In Table 3 steady state crack velocity v_{ss} and steady state fracture toughness K_{Iss} have been included from part I of this study [1]. Also, the overall surface roughness values are plotted against fracture toughness values in Fig. 6. These do not show any obvious correlation between the quantities. This lack of correlation between Ra and K_{Iss} is due to the dominant contribution of particles and/or particle footprints present on the fractured surface to the overall roughness. Hence, an alternative parameter is essential for providing a consistent explanation.

Table 2 shows experimentally measured roughness parameters, Ra_x, Ra_z and average roughness Ra for strongly bonded particles. Again, the roughness values are slightly but consistently higher in the transverse direction compared to the longitudinal direction. More importantly, as in case of weakly bonded particles, longitudinal, transverse, and overall roughness parameters increase with particle size. From Fig. 6 it can be seen again that Ra does not provide a unique correlation

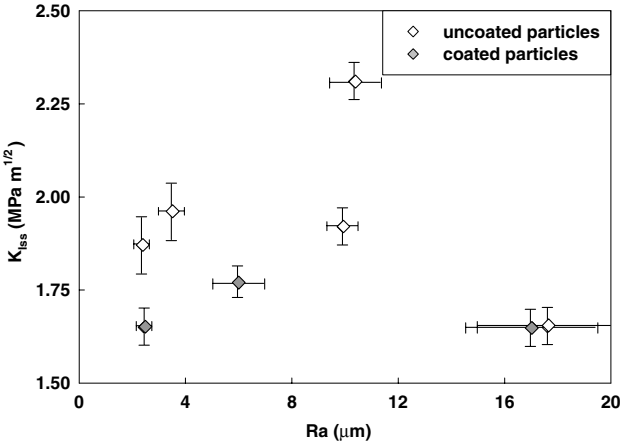

Fig. 6. Steady-state fracture toughness variation as a function of overall surface roughness for different filler particle sizes.

Table 3
Fracture and roughness parameters for different particle sizes and filler–matrix strengths at $V_f = 0.1$

Average particle size (μm)	Weakly bonded particles				Strongly bonded particles			
	Crack velocity, v^*_{ss} (m/s)	Fracture toughness, K^*_{Iss} (MPa $\sqrt{m}$)	Measured roughness, Ra (μm)	$\frac{Ra_f}{\sqrt{D}}$	Crack velocity, v^*_{ss} (m/s)	Fracture toughness, K^*_{Iss} (MPa $\sqrt{m}$)	Measured roughness, Ra (μm)	$\frac{Ra_f}{\sqrt{D}}$
203	310	1.67	17.61	0.45	312	1.65	17.04	0.41
71	300	1.92	9.90	0.71	–	–	–	–
35	290	2.31	10.33	1.42	320	1.77	6.00	0.69
11	345	1.96	3.52	0.88	375	1.65	2.42	0.55
7	370	1.87	1.97	0.75	–	–	–	–

Subscript ss denotes "steady state", * denotes data from [1].

with K_{Iss} even for strongly bonded particles. Usefulness of overall surface roughness hence requires that contribution of particle size to the surface roughness be duly accounted for prior to correlating macro-measurements with micro-measurements pertaining to the fracture surface.

Comparing Ra_x, Ra_z and Ra in Tables 1 and 2 for respective particle sizes, it can be noted that roughness values are consistently higher for each case of weakly bonded particles when compared to the silane treated ones. Maximum increase in roughness values are for the case of 35 μm particles, with weakly bonded particles showing in excess of 70% increase in average roughness compared to the one for strongly bonded particles. Similar comparison between weakly and strongly bonded particles of 11 μm size and 203 μm size show ~45% and negligible increase in Ra, respectively.

3.2. Potential toughening mechanisms and surface roughness

It can be seen from the micrographs that filler particles are unbroken in all composites and the crack always travels through the matrix material. When the crack front encounters filler particles during crack propagation, it interacts with the filler phase in one of the following two ways depending upon filler–matrix interface strength. If filler–matrix interface is strong, crack tends to deviate from its path and bow around or tilt between rigid filler particles. Bowing around the particles or crack tilting gives rise to mixed mode-I and -II fracture, while the crack twisting between particles results in mixed mode-I and -III [10,11] condition. On the contrary, if filler–matrix interface is weak, cleavage fracture can be noticed in the interparticle region with particle footprints left behind by the propagating crack (see Fig. 1). Clearly the matrix surrounding the filler particles is separated as the crack front encounters weaker filler–matrix interface. In this process the propagating crack front bows out wherever it meets the filler phase while being blunted at discrete locations along the front. Such a crack would experience lowering of stress intensification and needs additional energy to overcome the blunting effect to re-initiate and propagate further. These intermittent stalling of crack growth in the form of blunting and re-initiation gives rise to lower average crack velocity. The same can be readily noticed by comparing the steady state crack velocities in Table 3, where the crack velocities are always higher for strongly bonded particles relative to weakly bonded particles of similar sizes. Weaker filler–matrix interface could also act as a distribution of crack attractors for a propagating crack front. Hence the crack tends to meet-up with the nearest possible filler–matrix interface in its neighborhood during propagation, which again gives rise to zig–zag crack propagation instead of relatively straight/smooth fracture path. These are schematically shown in Fig. 7. The above mentioned phenomena vary

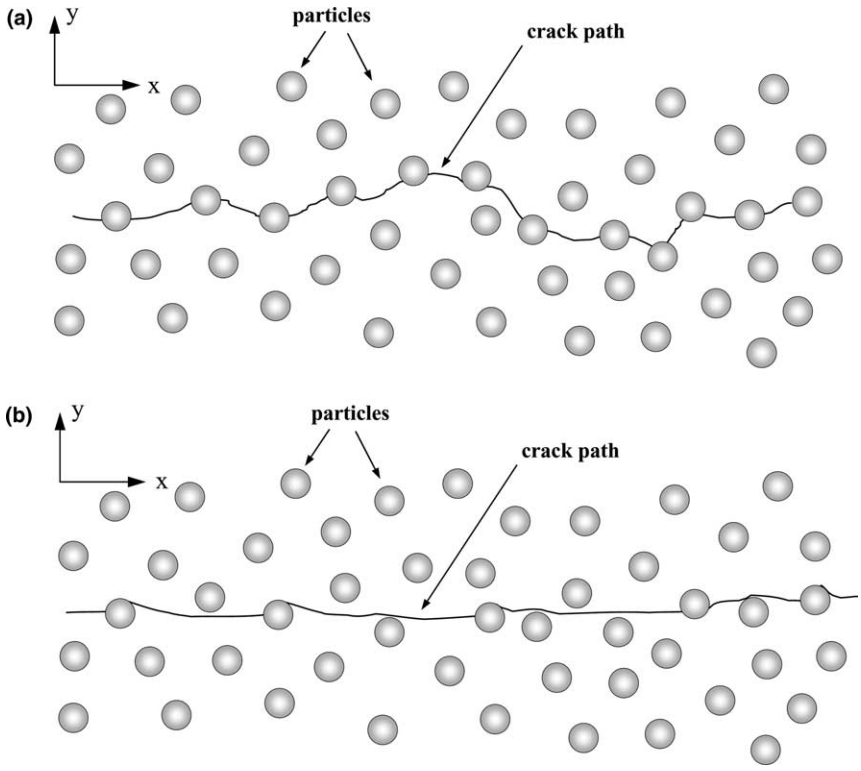

Fig. 7. Schematic showing potential crack growth pattern: (a) weakly bonded particles and (b) strongly bonded particles.

the microscopic surface features giving rise to higher surface roughness and hence the macroscopic fracture toughness. This can be noticed by comparing roughness and fracture toughness values in Table 3 between weakly and strongly bonded particles. The values are consistently higher for weakly bonded case of similar particles sizes.

From the above analysis it is clear that different mechanisms affect fracture toughness and surface roughness based on filler–matrix interface strength. In the micrographs "tail lines" emerging from the particles/cavities or within matrix material show direction of crack propagation. These lines are also indicative of the magnitude of surface tortuosity and crack twisting during fracture. The formation of tail lines can be explained with the help of schematics shown in Fig. 8. In the case of strongly bonded particles tail lines appear more often in the matrix material between particles (see Fig. 1(b), (d), and (f)). From the schematic in Fig. 8(a) it can be seen that when angle of twist ϕ reaches its maximum value ϕ_{max} (Fig. 8(a.iii)), crack front starts to propagate at different elevations (different values of y on x–z plane). This results in tail lines in the form of extra surface in the matrix material between the particles (Fig. 8(a.iv)). Unlike strongly bonded fillers (Fig. 8(b)), in weakly bonded particles tail lines appears to have been generated at the particles or particle footprints (see Fig. 1(a), (c), and (e)) by a slightly different mechanism. As discussed previously, weaker filler–matrix interface acts as a crack attractor, hence the crack front goes through the particle or particle footprint as shown in Fig. 8(b.i). When the angle of twist reaches its maximum value (Fig. 8(b.iii)), tail lines emerge from two neighboring particle sites (Fig. 8(b.iv)). It is clear that tail lines create extra surface, dissipating additional energy. Also the surface features are affected and surface roughness increases. It can be further noticed in the micrographs that tail lines are more prominent in weakly bonded particles when compared to the strongly bonded ones. This suggests that crack twisting has occurred more often in weakly bonded particles giving rise to higher surface roughness. This can be verified by comparing average roughness values in Tables 1 and 2 for respective particle sizes.

As noted from the results, 35 μm particles show maximum fracture toughness and fracture-induced roughness values. Further increase or decrease in particle size decrease both of these parameters. This behavior can be noticed both in weakly and strongly bonded particles, suggesting that the same phenomenon is responsible for an optimum particle size in both. Previously described tail lines and crack twisting in strongly and weakly bonded cases explain this. Fig. 8 shows crack twisting and formation of tail lines when the angle of twist ϕ reaches its maximum value ϕ_{max}. The random distribution of particles for 10% volume fraction is optimum for 35 μm particles, which gives an average ϕ nearly equal to maximum possible ϕ_{max}. Further increase in particle size increases the inter-particle separation l for constant volume fraction V_f (see Eq. (4)) increasing the probability of crack travelling through the matrix material. Hence average ϕ decreases as the particle size increases relative to the optimum value. On the other hand, when particle size decreases relative to the optimum size, inter-particle separation distance l decreases. More randomly distributed smaller particles per unit volume reduces the difference in elevations (in y-direction) between neighbouring particles (see Fig. 8), suggesting lower angle-of-twist. Also the smaller particle diameter gives rise to smaller angle-of-twist if neighbouring particles are at the same elevation. All these decrease the average ϕ. Hence it can be said that the optimum particle size seen in the experiments is primarily due to crack twisting. It should be pointed out, however, that the inter-particle separation distance l also depends on volume fraction of filler particles. This suggests that it is quite possible to see the deviation in optimum particle size from 35 μm to others for different volume fractions. This needs to be investigated by a study involving various particle sizes as well

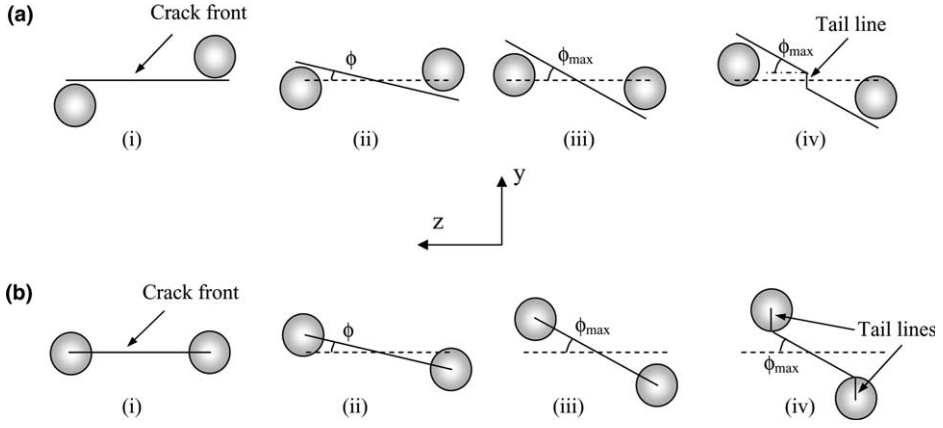

Fig. 8. Schematic showing different crack front twisting mechanisms in case of: (a) strongly bonded particles and (b) weakly bonded particles.

as different volume fractions, and will not be attempted here.

4. Linkage between macro- and micro-measurements

4.1. Fracture toughness–surface roughness relation excluding particle-size effect

Attempts to relate optically measured fracture toughness to surface roughness parameters are described next. As noted earlier, experimentally measured overall roughness values do not reflect a true linkage of fracture toughness to roughness parameters since roughness values are skewed by filler phase material. Therefore the component of roughness due to particle size needs to be isolated from the one due to the actual fracture process. This can be accomplished by nondimensionalizing the overall roughness values appropriately. An obvious question that arises is, what parameter/value should be used for nondimensionalizing? Using fracture toughness and surface roughness parameters of matrix material to nondimensionalize is inappropriate since the elastic properties of unfilled epoxy are different from the filled ones (see Table 1 in part I [1]). Thus, one needs to nondimensionalize using the ones of same elastic characteristics, thereby avoiding the influence of extraneous parameters. It should be noted here that very little effect of particle size is noticed on measured fracture toughness in case of strongly bonded filler. Based on this, it can be safely assumed that fracture toughness differences are negligible when particle–matrix interfaces are ideally bonded. Hence properties/parameters for the case of strongly bonded particles can be used to nondimensionalize the respective fracture and roughness parameters of various weakly bonded particle sizes. This would eliminate the particle size effect altogether and isolate the particle–matrix strength effects only. Fig. 9 shows the percentage increase in average roughness as a function of percentage increase in fracture toughness, respectively, for weakly bonded particles relative to strongly bonded particles for each particle size. Interestingly, the plot shows a simple linear variation for all three particle sizes considered in this study. Thus, a linear dependence of surface roughness on dynamic fracture toughness of glass-filled epoxy is demonstrated when particle size effect is "excluded".

4.2. Fracture toughness–surface roughness correlation

The next task is to correlate fracture toughness and surface roughness in the presence of different particle sizes and different filler–matrix adhesion strengths. As a first step, fracture toughness of the composite is expressed as,

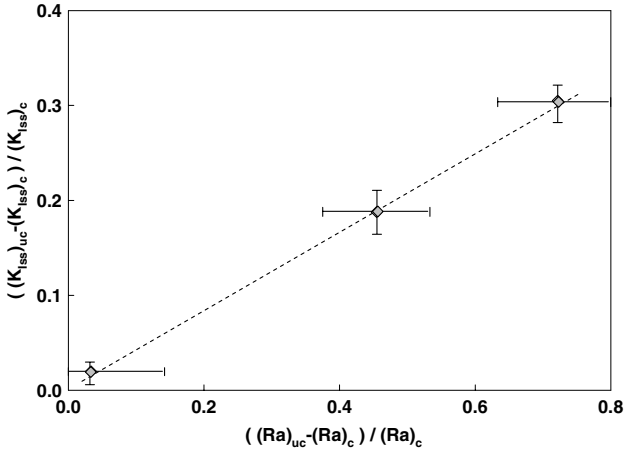

Fig. 9. Fracture toughness-surface roughness dependence excluding particle size effect (subscripts: ss, steady-state; uc, uncoated particles; c, coated particles).

$$K_{\mathrm{I}} = K_{\mathrm{Im}} + \Delta K_{\mathrm{I}}, \tag{16}$$

where K_{I} is overall fracture toughness of the composite, K_{Im} is the fracture toughness of unfilled matrix and ΔK_{I} is the change in fracture toughness due to the reinforcement. The total energy dissipation during the fracture process can be related to various parameters such as filler particle size, filler–matrix adhesion, surface morphology, critical strength of matrix material and so on, by considering various processes – breaking matrix constraints due to filler particles, driving the crack forward, creating the new surfaces, etc., in which energy is consumed.

Let us first consider the energy used in overcoming the matrix constraints due to filler particles. It can be seen from the micrographs that the crack invariably travels through the matrix material and particles are not fractured in these composites. When the crack propagates through the matrix material surrounded by the filler particles, the matrix is relatively shielded from the far-field stresses and experiences a reduced stress intensification at crack tip. As a result the critical value of far-field stresses for fracture increases in the presence of filler particles. Let $\sigma_{\mathrm{c}}^{\mathrm{m}}$ and $\sigma_{\mathrm{c}}^{\mathrm{f}}$ be the critical far-field stresses required for fracture in the absence and presence of filler particles, respectively. Then, the additional energy required to overcome the effect of filler particles can be assumed to be some function of $\Delta\sigma_{\mathrm{c}} = \sigma_{\mathrm{c}}^{\mathrm{f}} - \sigma_{\mathrm{c}}^{\mathrm{m}}$. Clearly $\Delta\sigma_{\mathrm{c}}$ depends on particle volume fraction. In the absence of particle agglomeration, the higher the filler volume fraction the greater will be the matrix constraint and crack tip shielding, and hence the higher $\Delta\sigma_{\mathrm{c}}$. Another important parameter which affects the constraint is inter-particle separation distance l. One can presume without much difficulty that the smaller the inter-particle l, the larger will be the matrix constraint

and crack tip shielding. Combining both factors, the increase in energy dissipation due to these and hence ΔK is proportional to $(\Delta\sigma_c)^p/l^q$. As per Eq. (4), two aspects namely particle size and volume fraction of the filler particles affect inter particle distance. Hence using Eq. (4), for constant volume fraction, ΔK can be written as,

$$\Delta K \propto (\Delta\sigma_c)^p/D^q, \tag{17}$$

where p and q are positive real constants and D is the particle size.

Now let us consider the energy component used in creating new surfaces, which is reflected in its effect on fracture surface roughness. As noticed earlier, glass-filled epoxy with both weakly and strongly bonded particles show increasing average roughness with particle size. This increasing trend, however, is not reflected in the optically measured fracture toughness. From roughness analysis in Section 2.2, it is quite evident that average roughness is a cumulative effect of roughness due to energy dissipation during fracture and the roughness due to the presence of particles on the fracture surface. Clearly the effect of particle-related roughness Ra_p increases with particle size. Based on a simple model, Ra_p has been calculated to be a function of particle size and volume fraction (see Section 2.2.1). Roughness induced by the fracture process or, fracture-induced roughness Ra_f, can be filtered out from total roughness Ra by algebraically subtracting Ra_p from Ra. Hence ΔK can be considered as some function of Ra_f. Assuming,

$$\Delta K \propto (Ra_f)^r, \tag{18}$$

where r is another positive real number. Here it should be noted that the effects of filler–matrix adhesion will be reflected in the surface roughness. Hence an extrinsic parameter to represent filler–matrix adhesion strength in the model is not necessary. That is, Ra_f incorporates all the details pertaining to crack tilting, twisting and blunting. Combining Eqs. (17) and (18) and using proportionality constant β, one can express ΔK as,

$$\Delta K = \beta\frac{(\Delta\sigma_c)^p}{D^q}Ra_f^r. \tag{19}$$

Further ΔK can be replaced in Eq. (16) by using Eq. (19) to get

$$K_I = K_{Im} + \beta\frac{(\Delta\sigma_c)^p}{D^q}Ra_f^r. \tag{20}$$

In Section 4.1 it has been demonstrated that increase in average surface roughness linearly varies with fracture toughness, which suggests that exponent r should be unity. On substituting for $r = 1$, and assuming that β and $\Delta\sigma_c$ are constants, Eq. (20) bares similarity to well known Hall–Petch relation [1] used for describing strengthening mechanism in crystalline solids. Guided by the possibility that Hall–Petch like behavior might also prevail in particle filled epoxy, the exponent q is anticipated to be 1/2, which results in,

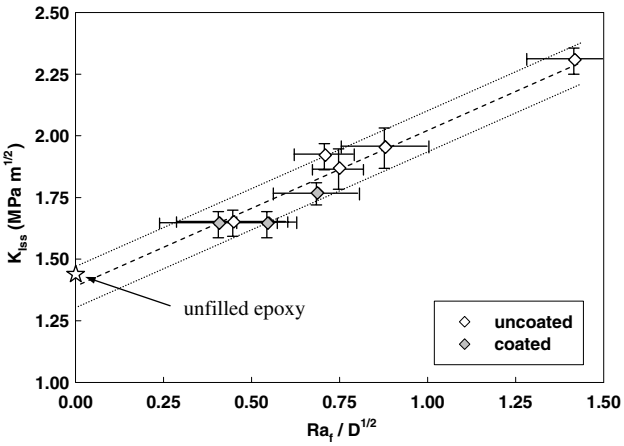

Fig. 10. Steady-state fracture toughness variation with fracture induced roughness and particle size of glass-filled epoxy composite.

$$K_I = K_{Im} + \beta\frac{(\Delta\sigma_c)^p}{\sqrt{D}}Ra_f. \tag{21}$$

Fig. 10 shows variation of dynamic fracture toughness K_{Iss} with $Ra_f/\sqrt{D}$ for both weakly and strongly bonded particles of various particle sizes. The linear variation between K_{Iss} and $Ra_f/\sqrt{D}$ clearly justifies a simple two parameters relationship given in Eq. (21). Quite interestingly the linear fit of the experimental data gives $K_{Im} \approx 1.4$ MPa$\sqrt{m}$. This value is close to the fracture toughness of unfilled epoxy extracted from the experiments, which is in the range of 1.4–1.6 MPa $\sqrt{m}$ (see part I of the study [1]). On the other hand, in case of unfilled epoxy, setting $\Delta\sigma_c = 0$ reduces Eq. (21) to $K_I = -K_{Im}$, further justifying the chosen form of the model. The model can be further refined by performing dimensional analysis on Eq. (21). The slope of a linear fit of data in Fig. 10 of constant slope shows $\beta(\Delta\sigma_c)^p = constant$. If β is chosen to be non-dimensional constant, p should have a value of unity, which in turn also justifies our prior assumption of $\Delta\sigma_c = constant$, for a constant V_f. Hence the model can be reshaped in its final form as,

$$K_I = K_{Im} + \beta\frac{\Delta\sigma_c}{\sqrt{D}}Ra_f. \tag{22}$$

[1] The presence of grain boundaries affect the deformation behavior of a material by serving as an effective barrier to dislocation motions. The yield strength of a polycrystalline material in the presence of grain boundaries is, $\sigma_{ys} = \sigma_i + k_y D^{-1/2}$, where σ_i is overall resistance of lattice to dislocation movement, k_y is the locking parameter which measures relative hardening contribution of grain boundaries and D is grain size [20].

5. Conclusions

Experiments have been performed to characterize particle size and filler–matrix adhesion effects on fracture surface parameters of glass-filled epoxy under impact loading conditions. Filler particles used in the experiments are uncoated and silane treated soda-lime glass spheres of mean dia. from 7 to 203 μm in diameter. Fracture surface is analyzed qualitatively using scanning electron microscopy and quantitatively by surface profiles obtained from a profilometer. Surface roughness is correlated successfully with steady state fracture toughness results reported in part I of this study [1]. The mechanisms affecting fracture and roughness parameters in the presence of various particle sizes and different filler–matrix adhesion strengths have been investigated. The results can be summarized as follows:

- Micrographs show strong filler–matrix interfacial strength in silane treated fillers. Cracks bow around rigid filler particles in case of strongly bonded particles while they readily intersect the filler when weakly bonded.
- Crack tilting and twisting are dominant mechanisms in strongly bonded particles while crack front twisting and crack tip blunting affect fracture toughness and surface roughness parameters in weakly bonded particles.
- Differences in the tail lines are also indicative of crack twisting during fracture in weakly and strongly bonded filler. More prominent tail lines in weakly bonded particles suggest higher crack twisting effect and hence higher roughness parameters as compared to strongly bonded ones.
- Crack tip blunting retards crack growth and lowers steady state crack velocity in weakly bonded particles. Weaker filler–matrix interfaces also act as distributed attractors to the propagating crack giving rise to higher surface roughness.
- Average surface roughness Ra is modeled as a sum of particle-related roughness Ra_p and fracture-induced roughness Ra_f. Ra_p is a function of particle size and volume fraction. Ra_f truly reflects the effect of differing fracture mechanisms involved.
- Ra is consistently higher for weakly bonded particles as compared to strongly bonded ones. Ra increases as particles size increases. However, this does not correlate with macroscopically measured fracture toughness for various particle sizes.
- Fracture toughness shows linear correlation with surface roughness when particle size and filler–matrix adhesion effects are factored out.
- A simple model is proposed for correlating fracture toughness, fracture-induced roughness and particle size. The quantity $Ra_f/\sqrt{D}$ has been found to be linearly varying with steady state dynamic fracture toughness.

Acknowledgements

Authors thank US Army Research Office for supporting this research through Grants DAAD-19-01-1-0414 and W911NF-04-1-0257 (Dr. Bruce LaMattina, Program Director). Also, enthusiastic support of Mr. Chris Smith, Technical Manager of Potters Industries, Inc., is gratefully acknowledged for providing the filler materials used in this research.

References

[1] Kitey R, Tippur HV. Role of particle size and filler–matrix adhesion on dynamic fracture of glass-filled epoxy. I. Macro-measurements. Acta Mater 2005, this issue. Doi:10.1016/j.actamat.2004.11.012.
[2] Cotterell B. Fracture propagation in organic glass. Int J Fract Mech 1968;4:209–17.
[3] Ravi-chandar K, Knauss WG. Experimental investigation into dynamic fracture: II. Microstructural aspects. Int J Fract 1984;26(1):65–80.
[4] Arakawa K, Takahashi K. Relationships between fracture parameters and fracture surface roughness of brittle polymers. Int J Fract 1991;48:103–14.
[5] Takahashi K, Kido M, Arakawa K. Fracture roughness evolution during mode I dynamic crack propagation in brittle materials. Int J Fract 1998;90:119–31.
[6] Sharon E, Gross SP, Fineberg J. Energy dissipation in dynamic fracture. Phys Rev Lett 1996;76(12):2117–20.
[7] Tandon S, Faber KT. Effects of loading rate on the fracture of cementitious materials. Cem Concr Res 1999;29:397–406.
[8] Issa AMo, Issa AMa, Islam MS, Chudnovsky A. Fractal dimension-a measure of fracture roughness and toughness of concrete. Eng Fract Mech 2003;70:125–37.
[9] Abell AB, Lange DA. Fracture mechanics modeling using images of fracture surfaces. Int J Solids Struct 1998;35:4025–33.
[10] Faber KT, Evans AG. Crack deflection process-I Theory. Acta Metall 1983;31(4):565–76.
[11] Faber KT, Evans AG. Crack deflection process-II Experiment. Acta Metall 1983;31(4):577–84.
[12] Davidson DL. Fracture surface roughness as a gauge of fracture toughness: aluminium-particulate SiC composites. J Mater Sci 1989;24:681–7.
[13] Kobayashi T, Shockey DA. FRASTA: A new way to analyze fracture surfaces, Part 1: Reconstructing crack histories. Adv Mater Process 1991;140(5):28–34.
[14] Kobayashi T, Shockey DA. Fracture analysis via FRASTA, Part 2: Determining fracture mechanisms and parameters. Adv Mater Process 1991;140(6):24–32.
[15] Komai K, Minoshima K, Ishii S. Recognition of different fracture surface morphologies using computer image processing techniques. Jpn Soc Mech Eng 1993;A36(2):220–7.
[16] Hao Y, Wang ZG, Tian JF. A quantitative investigation of fatigue fracture surfaces by using the Fourier transform method. Mater Sci Eng A 1993;161:195–200.
[17] Kobayashi T, Shockey DA. The relationship between fracture surface roughness and fatigue load parameters. Int J Fatigue 2001;23:S135–42.
[18] Fullman RL. Measurement of particle sizes in opaque bodies. Trans AIME J Met 1953(March):447–52.
[19] Lange FF, Radford KC. Fracture energy of an epoxy composite system. J Mater Sci 1971;6:1197–203.
[20] Hertzberg RW. Deformation and fracture mechanics of engineering materials. 4th ed. Wiley; 1996.